JMEPEG (2016) 25:3890–3895
DOI: 10.1007/s11665-016-2207-0

1059-9495/$19.00

The Influence of Zn Content on the Corrosion and Wear Performance of Mg-Zn-Ca Alloy in Simulated Body Fluid

Hua Li, Debao Liu, Yue Zhao, Feng Jin, and Minfang Chen

(Submitted January 28, 2016; in revised form May 15, 2016; published online July 11, 2016)

Mg-Zn-Ca alloy has been attracting increasing attention as a potential biodegradable implant material. In this paper, Mg-3Zn-0.2Ca and Mg-4Zn-0.2Ca alloys were prepared by means of vacuum melting and subsequent hot extrusion process. The influences of Zn content on the microstructure, mechanical properties, and corrosion and wear behavior of Mg-Zn-Ca alloys in simulated body fluid (SBF) were studied. The results show that with increased Zn content, the grain size and corrosion resistance were decreased, while the mechanical strength and wear resistance were increased, under both dry sliding and SBF-lubricated conditions. For the same Mg-Zn-Ca alloy, the wear loss rate under SBF lubrication was higher than dry sliding condition, indicating a strong corrosion-assisted wear effect of SBF to the Mg-Zn-Ca alloy.

Keywords corrosion resistance, mechanical properties, Mg-Zn-Ca alloy, wear resistance, Zn content

1. Introduction

Magnesium and magnesium alloys have attracted increasing attention as "smart" metal implant materials due to their suitable mechanical properties with bones, good biocompatibility, and biodegradability in physiological environment (Ref 1, 2). Currently, the major drawback of the magnesium alloys as implant materials is that they corrode too fast (Ref 3), this is because the Pilling-Bedworth (PB) ratio of 0.84 for the oxide layer (MgO) is less than 1 and the oxide layer cannot form a stable protection. Furthermore, in an aqueous medium, surface film formation on the magnesium and magnesium alloys usually accompanied by H_2 evolution, which will destroy the compactness of the surface film (Ref 3, 4). Magnesium and magnesium alloys corrode too fast in electrolytic and high chloride environments of the physiological system, losing their mechanical integrity before the completion of bone tissue healing. The rapid release of degradation products produces significant changes in the microenvironment of the implantation site and destroys the physiological balance of adjacent areas, raising the risk of disease and complication (Ref 5, 6).

The addition of alloying elements is an effective means to improve the mechanical strengths and corrosion resistance. It is well known that zinc is one of the most abundant nutritionally essential elements in the human body. For magnesium alloys containing zinc, a protected film containing zinc element will form on the surface of the alloy and this film can effectively protect the alloy to avoid further corrosion. Mg-Zn alloy has obvious precipitation hardening due to high solubility of the Zn element in magnesium. The addition of Zn to Mg results in a continuous increase in yield strength (YS) as Zn increases from 1 to 6 wt.%. However, the Zn content should be limited to 4 wt.% to achieve a good combination of mechanical properties and corrosion resistance (Ref 7). Mg-Zn binary alloy was developed with the aim of making a novel magnesium alloy with good biocompatibility, moderate degradation rate, and good mechanical properties (Ref 8). Another alloying element, Ca, is a major component of the human bone and can accelerate bone. Mg-Ca alloy does not induce toxicity in vitro cytotoxicity test and can gradually degrade in vivo within 90 days and accelerate new bone formation (Ref 9). Ca has excellent grain-refinement efficiency in magnesium due to its high growth restriction factor (GRF). The solubility of Cain Mg is only about 1.34 wt.% under equilibrium conditions. With increasing Ca content, coarse Mg-Ca brittle phase further precipitates along grain boundaries, which have a negative effect on the ductility of Mg alloy, and also accelerates the degradation due to galvanic corrosion (Ref 10). As reported, the addition of Zn in the Mg-Ca binary alloys can optimize their mechanical and degradation properties (Ref 11). Therefore, Mg-Zn-Ca alloy's application for degradable bone internal fixation has been interested in recent years (Ref 7, 12). In this paper, 3 and 4 wt.% zinc with 0.2 wt.% calcium were added to Mg matrix to fabricate the Mg-3Zn-0.2Ca and Mg-4Zn-0.2Ca alloys. A low strain rate was applied in the subsequent extrusion process to avoid hot tear. Microstructure, mechanical properties, and biocorrosion properties of as-extruded Mg-Zn-Ca alloys were investigated for a bone-implant compatibility check. There is inevitably some degree of micromovement at the bone-implant interface in vivo, and wear debris causes inflammation and other side effects. The interface between an implant and its surrounding tissues represents a friction pair. So the friction features are especially important for bone-implant compatibility. When magnesium alloys implanted in vivo, the corrosion process will also have a impact on the wear behavior in body fluid environment. So far, few work has been done to study the corrosion and wear behavior of Mg alloy in the service environment (Ref 13). In this work, the corrosive wear behavior of the as-extruded Mg-*x*wt.%Zn-0.2 wt.%Ca (x = 3.0,4.0, respectively) alloys in simulated body fluid (SBF) were also studied.

Hua Li, Debao Liu, and **Minfang Chen**, School of Materials Science and Engineering, Tianjin University of Technology, Tianjin 300384, China; **Yue Zhao**, School of Materials Science and Engineering, Tianjin University of Technology, Tianjin 300384, China and School of Mechanical, Materials & Mechatronic Engineering, University of Wollongong, Wollongong, NSW 2522, Australia; and **Feng Jin**, Tianjin Sannie Bioengineering Technology Co. Ltd, Tianjin 300384, China. Contact e-mail: debaoliu@126.com.

2. Experimental Procedure

2.1 Sample Preparation

High-purity Mg (99.99%), high-purity Zn (99.999%), and a high-purity Mg-30 wt.% Ca master alloy were used to prepare Mg-3Zn-0.2Ca and Mg-4Zn-0.2Ca alloys. Melting was conducted at 720 °C in an induction furnace protected by 99.999% Argon. The melt metal was first given a mixing treatment and then cast in a copper mold. The analyzed chemical compositions of the prepared alloys by infrared spectrometry are given in Table 1.The ingot of 60-mm dimension was extruded at 300 °C into a bar of 10 mm in diameter, giving an extrusion ratio of 36:1. Aging treatment was carried out for the extruded specimens at 170 °C for 24 h.

2.2 Characterization of Microstructure

The microstructure of the alloy was examined by optical microscopy (OM). The grain structure was revealed by chemical etching using 10% nitric acid methanol solution and a solution of picric aid (2.75 g), acetic acid (2.5 ml), ethanol (45 ml), and deionized water (5.0 ml). Phase identification was carried out using x-ray diffraction (XRD, Rigaku D/max/2500PC).

2.3 Mechanical Properties Test

Following the specifications in GB/T16865-2013 standard, tensile specimens with a gage length of 25 mm and a diameter of 5 mm were machined from the as-extruded bars. Tensile strength was tested on an electronic universal testing machine with the tensile rate 20 mm/min. At least three samples were tested for each condition. The hardness of the specimens was measured after mechanical polishing on an HMV-2T Vickers microhardness tester, with a load of 0.1 kg for 10s.

2.4 Electrochemical Test

The samples of 8 mm in diameter and 3 mm in thickness were mounted in epoxy resins with an exposed area of 0.5 cm^2. The surface was ground on 500 and 2500 grit SiC paper and polished with a 1-μm diamond paste before ultrasonic cleaning in absolute ethanol and deionized water. The electrochemical tests were performed using a three-electrode configuration. A saturated calomel electrode (SCE) and a graphite electrode were used as the reference and counter electrode, respectively, and the working electrode was the magnesium alloy sample. In the polarization test, the working electrode was first immersed in the SBF for 20 min and then the polarization curve was measured at a scanning rat of 0.01 mV/s. Electrochemical impedance spectroscopy (EIS) analysis was performed at the open circuit potential with the frequency varied from 100 KHz to 0.1 Hz.

2.5 Immersion Test

According to ASTM G31-72 (Ref 14), immersion tests were performed using a water bath at 37 °C in the SBF with an initial pH value of 7.4. The solution was replaced every 48 h to simulate the metabolic environment of human body. Samples were immersed in the SBF solution at 37 ± 1 °C for 3 days. Then, the samples were ultrasonically cleaned in deionized water. The mass of the samples was measured before and after the immersion by an electronic balance with an accuracy of 0.1 mg. To calculate the mass loss, the immersed samples were cleaned using a mixed solution of 5 g $K_2Cr_2O_7$ + 10 ml H_2O + 90 ml H_2SO_4 to remove the surface corrosion products, then rinsed with ethanol, dried in air, and finally weighed. The corrosion rates were calculated by weight loss according to ASTM-G31-72:

$$\text{Corrosion rate} = (K \times W) / (A \times T \times D), \quad \text{(Eq 1)}$$

where the coefficient $K = 8.76 \times 10^3$, W is the weight loss, A is the initial surface area exposed to the SBF, T is the immersion time, and D is the standard density of tested materials. Three parallel samples were used for each condition and the results were averaged. The surface morphologies after immersion were observed using SEM.

2.6 Wear Test

The wear tests were carried out in a coating friction and wear testing machine with a pin-on-disk contact configuration as shown in Fig. 1. The counterface was a stainless steel disk with a diameter of 80 mm. The pin samples were machined with a diameter of 8 mm, height of 15 mm. Before testing, the pin samples and steel disk were ground with SiC paper up to

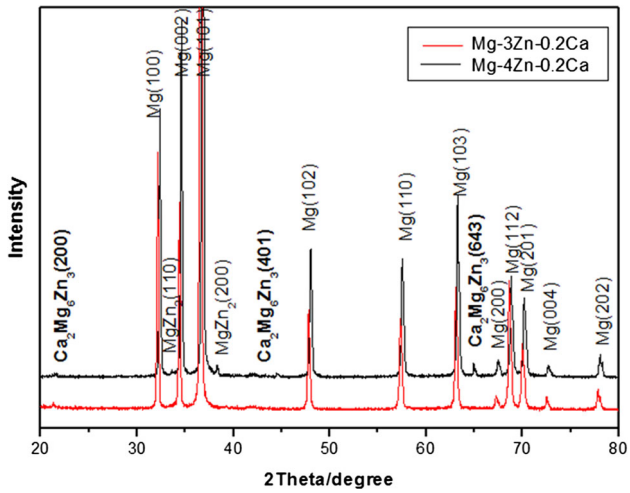

Fig. 1 XRD pattern of Mg-3Zn-0.2Ca and Mg-4Zn-0.2Ca alloy

Table 1 Chemical compositions of the two Mg-Zn-Ca alloys

Alloy	Zn (wt.%)	Ca (wt.%)	Al (wt.%)	Fe(wt.%)	Mg (wt.%)
Mg-3Zn-0.2Ca	3.0345	0.1982	0.1302	0.0096	0.008
Mg-4Zn-0.2Ca	3.9635	0.2013	0.1125	0.0095	0.011

2000 grit, followed by ultrasonic cleaning in anhydrous ethanol and deionized water for 10 min followed by drying in hot air. The tests were carried out under applied loads of 3Nat a constant rotational velocity of 200 r/min (linear speed of 0.65 m/s), with the sliding time of 30 min. The tests were performed under SBF lubrication and dry sliding condition, respectively. After the tests, the magnesium alloy samples were ultrasonically cleaned in anhydrous ethanol and dried in hot air. The samples were weighed before and after the test in order to determine the mass loss during test. All the tests were repeated three times at the same condition and the result was averaged.

The wear rate of the magnesium alloy was determined by the Archard's law (Ref 15):

$$V/L = KW/H, \quad \text{(Eq 2)}$$

where V is the wear volume, L is the sliding distance, W is the applied load, H is the hardness of the magnesium alloy, and K is the Archard's constant.

In order to confirm the wear mechanisms, the worn surfaces of the magnesium alloy under different condition were examined by SEM.

3. Results and Discussion

3.1 XRD and Microstructure Analysis

The XRD pattern of the extruded Mg-3Zn-0.2Ca alloy is presented in Fig. 1, which shows that the main constituent phases of the prepared Mg-4Zn-0.2Ca alloy are α-Mg and some second phases such as $MgZn_2$ and $Ca_2Mg_6Zn_3$, respectively. It is found that there are no distinct $MgZn_2$ and $Ca_2Mg_6Zn_3$ phases that can be identified by XRD in Mg-3Zn-0.2Ca alloy, indicating that the amount of these brittle phases was lower in comparison with the Mg-4Zn-0.2Ca alloy.

Figure 2 displays the microstructures of the extrusion and aging treated Mg-*x* wt.%Zn-0.2 wt.%Ca alloys with different Zn content. It can be seen that the average grain size became finer with increasing Zn content. During the process of the solidification, the excessive Zn content were rejected and concentrated ahead of the primary α-Mg phase and would limit the growth of α-Mg. As a result, with increasing Zn content, grain size became finer.

3.2 Mechanical Properties

Fig.3 presents the tensile stress-strain curve of the extruded Mg-*x*wt.%Zn-0.2 wt.%Ca alloy. Detailed results of mechanical properties tests are given in Table 2. The results show that with increasing Zn content, the yield and tensile strength improved, however, the elongation decreased slightly. The maximum solid solubility of Zn element in magnesium matrix is 6.2 wt.% according to Mg-Zn phase diagram and with decreasing temperature, only 1 wt.% Zn element remains soluble in Mg matrix and plays the role of solid solution strengthening and the excessive Zn content will form $MgZn_2$ or $Ca_2Mg_6Zn_3$ phases. With the increasing Zn content, the amount of intermetallic compound phases increases and exerts the effect of dispersion

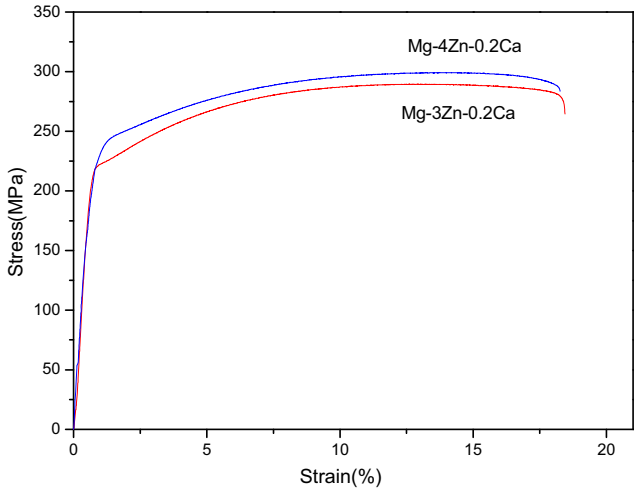

Fig. 3 Tensile Stress-strain curves of extruded Mg-3Zn-0.2Ca and Mg-4Zn-0.2Ca alloy

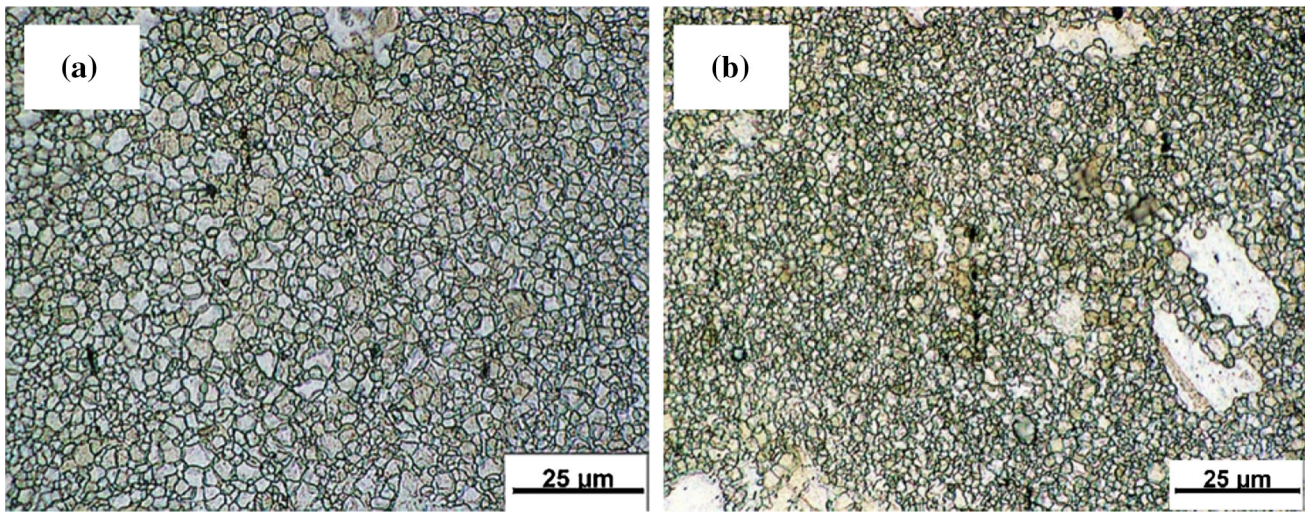

Fig. 2 Optical micrograph(OM) microstructures of the Mg-Zn-Ca alloys with different Zn content. (a) Mg-3Zn-0.2Ca alloy (b) Mg-4Zn-0.2Ca alloy

Table 2 Mechanical properties of the extruded Mg-Zn-Ca alloy

Alloy	Yield strength (MPa)	UTS (MPa)	Elongation (%)
Mg-3Zn-0.2Ca	224	273	18.5
Mg-4Zn-0.2Ca	243	295	18

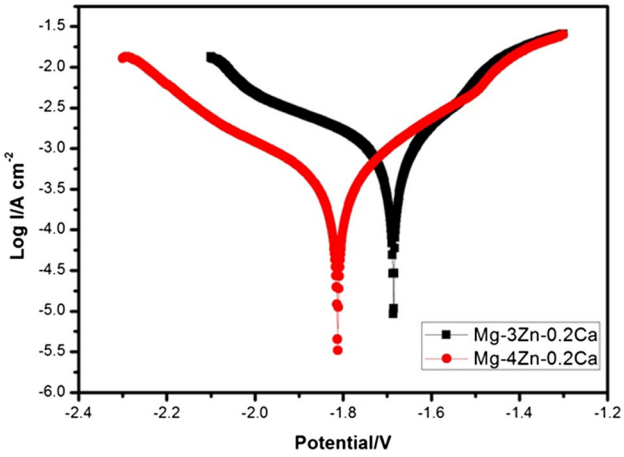

Fig. 4 Polarization curves of Mg-Zn-Ca alloys in SBF

strengthening. Therefore, the strength and hardness of Mg-Zn-Ca alloys improves with the increasing Zn content.

3.3 Electrochemical Characterization

Figure 4 shows the polarization curves of the extrusion and aging treated Mg-Zn-Ca alloys with different Zn content. It can be seen that with the increasing Zn content, the corrosion potential decreases. The corrosion potential reflects a combination of the electrochemical reactions at the interface between sample and the SBF solution. This indicates that the corrosion susceptibility increased with the increasing Zn content. The main corrosion mechanism of magnesium alloy in SBF is galvanic corrosion. The main intermetallic phases in Mg-Zn-Ca alloy such as $MgZn_2$ and $Ca_2Mg_6Zn_3$ phases are cathodic, so with the increasing content of zinc, the amount of intermetallic phase increased, resulting in the corrosion susceptibility being increased. Meanwhile, the average grain size of Mg-Zn-Ca alloy decreases with the increasing Zn content. Mg alloy is especially susceptible to corrosion attack at defect sites such as grain boundary due to that the atomic arrangement at these sites is looser and disordered. Hence, the grain refinement increased the surface activity of magnesium alloy, which accelerates the occurrence of corrosion (Ref 16).

3.4 Immersion Experiments

Figure 5 presents the weight loss and corrosion rate of the Mg-Zn-Ca alloys with different Zn content in the SBF. The results clearly show that the weight loss increased with increasing immersion time and Zn content. The weight loss rate was high in the first four hours and then gradually reached

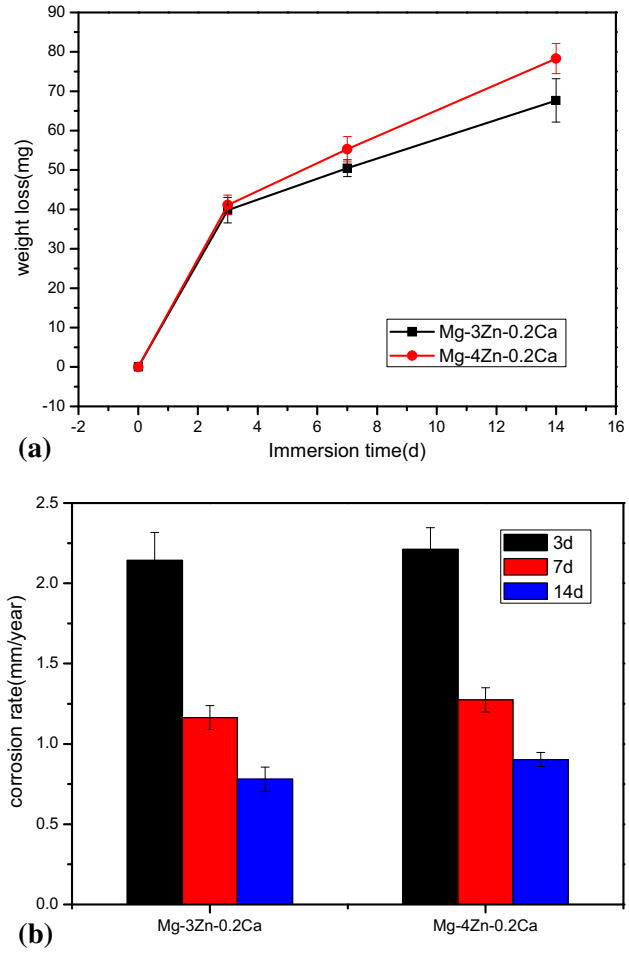

Fig. 5 Weight loss and corrosion rate of Mg-Zn-Ca alloys with different Zn content immersed in SBF. (a) weight loss, (b) corrosion rate

a stable stage upon further immersion. In our experiment, when the fresh surfaces of magnesium alloys were exposed to the SBF solution, chemical dissolution and electrolyte penetration resulted in a spontaneous corrosion process on the entire surface which led to fast degradation of the sample surface. The anodic dissolution of Mg matrix forms a magnesium hydroxide film on the surface of the alloys. However, the film was porous. The surrounding solution could continuously penetrate through the porous film and react with the inner alloy. Previous researches showed that the main causes of magnesium alloy corrosion were pitting corrosion, since galvanic coupling formed between the secondary phases and the matrix (Ref 2). And the uniformity of microstructure and composition could effectively weaken the effect of galvanic coupling. The more stable and protective the film formed on the surface of the alloy, the higher the value of the corrosion potential the alloy shows. Thereby, it is believed that relatively stable and protective film was formed on the surface of alloy with the Zn content relatively lower, resulting a lower weight loss.

3.5 Tribological and Wear Properties

Figure 6 presents weight loss of the Mg-Zn-Ca alloys with different Zn content under dry sliding and SBF lubrication. It

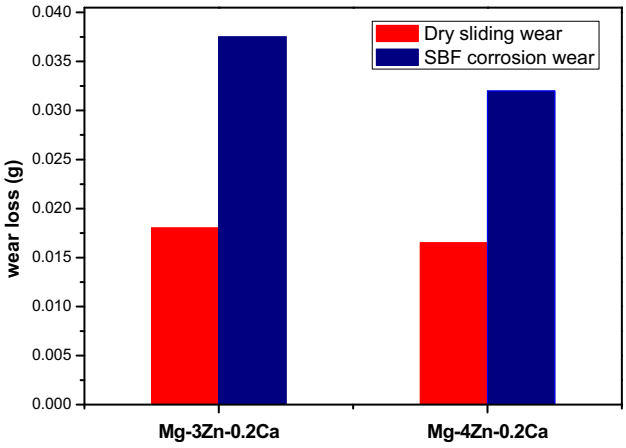

Fig. 6 Wear loss of the Mg-Zn-Ca alloys with different Zn content under dry sliding and SBF lubrication condition

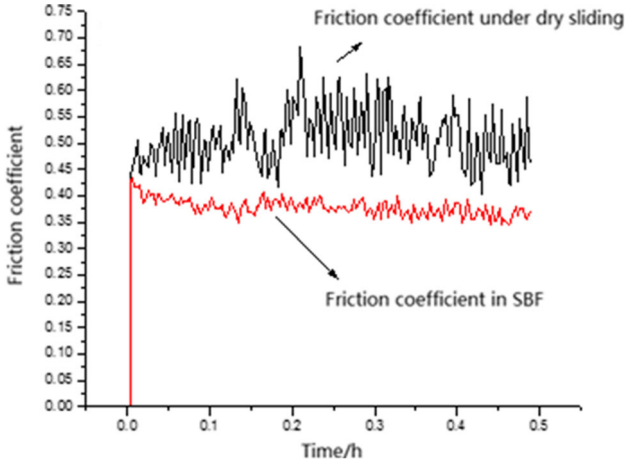

Fig. 7 Friction coefficient friction variation trend with the time of the Mg-3Zn-0.2Ca alloy under dry sliding and SBF condition

can be seen that the weight loss of Mg-Zn-Ca alloys decreased with increasing Zn content. With the increasing Zn content, the hardness of the alloy increased, which led to the improvement of the wear resistance. For the same alloy, the wear loss under the dry sliding condition is still lower than that under the SBF lubrication condition, indicating that the corrosion effect of SBF was stronger than its lubrication effect during the process of friction.

There are two effects of SBF on the wear behavior of magnesium alloy. Firstly, SBF has a lubrication action which is beneficial to decrease the friction coefficient. Figure 7 shows the friction coefficient variation trend with the time. It can be seen that the friction coefficient under SBF lubrication is lower than that under dry sliding condition. When under dry sliding condition, the friction heat can have a softening effect to magnesium alloy. As a result, the adhesion of the worn surfaces of magnesium alloy exhibited high friction coefficient under dry sliding condition. With regard to friction coefficient, lubrication action of SBF is beneficial for reducing the wear loss. On the other hand, SBF has a corrosion effect on the magnesium alloy. Once the magnesium alloy is in contact with SBF, electrochemical reaction will immediately take place. The corresponding anodic and cathode reactions are given in Eq 3 and 4 (Ref 6):

$$\text{Anodic reaction}: \quad Mg \rightarrow Mg^{2+} + 2e^{-} \qquad \text{(Eq 3)}$$

$$\text{Cathode reaction}: \quad 2H_2O + 2e^{-} \rightarrow H_2(g) + 2OH^{-} \qquad \text{(Eq 4)}$$

$$\text{Total reaction}: \quad Mg + H_2O \rightarrow Mg(OH)_2 + H_2(g). \qquad \text{(Eq 5)}$$

This electrochemical reaction mainly includes two mechanisms. On one hand, different phases in magnesium alloy caused the galvanic corrosion of the α-Mg matrix. On the other hand, electrochemical reaction between magnesium alloy and stainless steel counterface also result in the corrosion of α-Mg matrix. Moreover, the protection film formed by corrosion would be damaged due to mechanical wear, which resulted in rapid corrosion and flaking wear debris would also cause abrasive wear. Therefore, from the corrosion effect of SBF point of view, higher wear loss was caused by the introduction of SBF. According to the result shown in Fig. 6, the corrosion

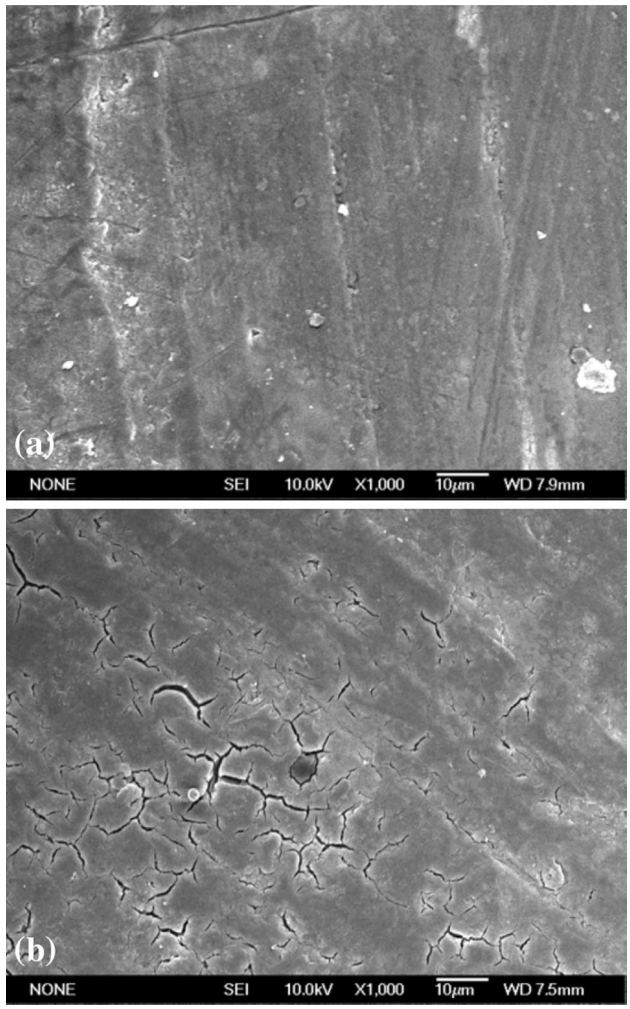

Fig. 8 Surface wear morphology of the Mg-3Zn-0.2Ca alloy under dry sliding condition and SBF condition. (a) under dry sliding condition (b) in SBF condition

effect of SBF was stronger than its lubrication effect during the process of friction and resulted in a significant wear loss increase in the SBF-added wear tests.

Figure 8(a) shows the worn surface SEM images of the Mg-3Zn-0.2Ca alloy under dry sliding condition. Some slight shallow grooves can be seen on the wear surface under dry sliding condition, indicating that the main wear mechanism is abrasive. Figure 8(b) shows the worn surface of the Mg-3Zn-0.2Ca alloy under SBF lubrication condition. There were no obviously grooves can be seen on the wear surface of the magnesium alloy, however, some cracks can be found. During the process of friction under SBF-added condition, the magnesium alloy was vulnerable to scratch under load, resulting the magnesium alloy being easily corroded and aggravating the wear of the magnesium alloy.

4. Conclusions

The microstructure, mechanical properties, and corrosion and wear behavior of biodegradable Mg-3Zn-0.2Ca and Mg-4Zn-0.2Ca alloy were investigated and the following conclusions can be drawn.

(1) With the increasing Zn content, the grain size, was refined, the yield and ultimate tensile strengths were slightly improved, and the wear resistance increased, while the corrosion resistance decreased both under dry sliding and SBF lubricated conditions.
(2) The friction coefficient of the sliding pair under SBF was obviously lower than that under dry sliding condition. However, the wear rate of Mg-Zn-Ca alloy under SBF lubrication was higher than that under the dry sliding condition, indicating that the corrosion effect of SBF was more predominant than its lubrication effect during the process of friction.

Acknowledgments

The authors are grateful for the supports from the National Natural Science Foundation of China (No. 51271131) and key projects supported by Tianjin Science and Technology (15ZCZDSY00920)

References

1. Y.F. Zheng, X.N. Gu, and F. Witte, Biodegradable Metals, *Mater. Sci. Eng. R*, 2014, **77**, p 1–34
2. Yongjun Chen, Xu Zhigang, Christopher Smith, and Jag Sankar, Recent Advances on the Development of Magnesium Alloys for Biodegradable Implants, *Acta Biomater.*, 2014, **10**, p 4561–4573
3. Andrej Atrens, Guang-Ling Song, Fuyong Cao, Zhiming Shi, and Patrick K. Bowen, Advances in Mg Corrosion and Research Suggestions, *J. Magnes. Alloys*, 2013, **1**, p 177–200
4. G.-L. Song and Z. Xu, Effect of Microstructure Evolution on Corrosion of Different Crystal Surfaces of AZ31 Mg Alloy in a Chloride Containing Solution, *Corros. Sci.*, 2012, **63**, p 100–112
5. Nan Li and Yufeng Zheng, Novel Magnesium Alloys Developed for Biomedical Application: A Review, *J. Mater. Sci. Technol.*, 2013, **29**(6), p 489–502
6. M.P. Staiger, A.M. Pietak, J. Huadmai, and G. Dias, Magnesium and Its Alloys as Orthopedic Biomaterials: A Review, *Biomaterials*, 2006, **27**, p 1728–1734
7. B.P. Zhang, Y. Wang, and L. Geng, Research on Mg-Zn-Ca Alloy as Degradable Biomaterial, *Biomaterials—Physics and Chemistry*, R. Pignatello, Ed., In Tech, Zurich, 2011, p 183–204
8. Shaoxiang Zhang, Xiaonong Zhang, Changli Zhao, Jianan Li, Yang Song, Chaoying Xie, Hairong Tao, Yan Zhang, Yaohua He, Yao Jiang, and Yujun Bian, Research on an Mg-Zn Alloy as a Degradable Biomaterial, *Acta Biomater.*, 2010, **6**, p 626–640
9. X.N. Gu, Y.F. Zheng, Y. Cheng, S.P. Zhong, and T.F. Xi, In Vitro Corrosion and Biocompatibility of Binary Magnesium Alloys, *Biomaterials*, 2009, **30**, p 484–498
10. Zijian Li, Gu Xunan, Siquan Lou, and Yufeng Zheng, The Development of Binary Mg-Ca Alloys for Use as Biodegradable Materials Within Bone, *Biomaterials*, 2008, **9**, p 1329–1344
11. Du Hui, Zunjie Wei, Xinwang Liu, and Erlin Zhang, Effects of Zn on the Microstructure, Mechanical Property and Bio-corrosion Property of Mg-3Ca Alloys for Biomedical Application, *Mater. Chem. Phys.*, 2011, **125**, p 568–575
12. Y. Sun, B. Zhang, Y. Wang, L. Geng, and X. Jiao, Preparation and Characterization of a New Biomedical Mg-Zn-Ca Alloy, *Mater. Des.*, 2012, **34**, p 58–64
13. De-Bao Liu, Wu Bo, Xiao Wang, and Min-Fang Chen, Corrosion and Wear Behavior of an Mg-2Zn-0.2Mn Alloy in Simulated Body Fluid, *Rare Met.*, 2015, **34**(8), p 553–559
14. American Society for Testing and Materials. ASTM-G31-72: Standard Practice for Laboratory Immersion Corrosion Testing of Metals, *Annual Book of ASTM Standards.* American Society for Testing and Materials, Philadelphia, 2004
15. W.J. Huang, Q. Lin, and X. Zhang, Investigation of Tribological Properties of Magnesium Alloys Under Dry Sliding and Lubrication Condition, *J. Eng. Tribol.*, 2011, **225**(J1), p p35
16. Liu Debao, Liu Yichi, and Huang Yan, Effects of Solidification Cooling Rate on the Corrosion Resistance of Mg-Zn-Ca Alloy, *Progr. Nat. Sci*, 2014, **24**(5), p 452–457